Slender Body Theory and Optimization Procedures for Transonic Lifting Wing Bodies

N D Malmuth*
Rockwell International Science Center, Thousand Oaks California
C C Wu†
University of California at Los Angeles, Los Angeles, California
and
J D Cole‡
Rensselaer Polytechnic Institute Troy New York

Limit process asymptotic expansion has been applied to develop an unsteady equivalence rule for transonic speeds The rule characterizes the near field of the flow over a transonic body as harmonic in cross planes perpendicular to the freestream direction, and the far field as a pulsating nonlinear line source Derived ex pressions for the loading indicate a substantial simplification of the prediction problem for three dimensional transonic unsteady airfoils using the theory In another application of transonic slender body asymptotics, substantial reductions in wave drag have been demonstrated using a parametric inverse method The procedure leads to a nearly shockless equivalent body of revolution for a slender airplane using iteration concepts and elimination of jump discontinuities in the equivalent body surface pressure distributions Multiple constraints such as fixed volume and base area are satisfied in the method by correlation of the equivalent body geometry with features of the smoothed surface pressure distribution

Nomenclature

a = speed of sound fairing parameter amplitude parameter
A = angle of attack parameter α/δ (reduced body cross sectional area)
b = semispan in Fig 1 in units of δ
B = implicit functional representation of body shape [Eq (2)]
c = chord
C = body contour in cross flow plane
C_D = drag coefficient
C_p = pressure coefficient
D = drag
D_v = vortex drag
f_n = coefficient of sine harmonic in multipole expansion for ϕ^*
F = reduced body radius
F_1 = reduced base radius
g = second order term of near field expansion of far field
g_n = coefficient of cosine harmonic in multiple ex pansion for ϕ^*
K = transonic small disturbance parameter $=(1-M_\infty^2)/\delta^2$
K^* $=(1-M_\infty^2)/\delta^2 M_\infty^2$
L = lift
M_∞ = freestream Mach number
n = index delineating plunge or pitch ($n=0$ plunge $n=1$ pitch)
r_0 = normalized base radius in Fig 1 δ units
$\bar{r}$ $=\delta R/c$
r^* $=R/\delta c$
R = dimensional cylindrical coordinate shown in Fig 1
S = source strength function introduced in Eq (2)
$\tilde{t}$ $=2\delta UT/C$
T = dimensional time
U = freestream speed
v = cross flow velocity $\partial\phi/\partial r^*$
w = cross flow velocity $1/r^*(\partial\phi^*/\partial\theta)$
x $=X/c$
$X\ Y\ Z$ = dimensional Cartesian coordinate shown in Fig 1 (X parallel to freestream)
α = angle of attack shown in Fig 1
Γ = relaxation parameter
γ = specific heat ratio
δ = characteristic thickness ratio of body
θ = cylindrical polar coordinate shown in Fig 1
μ = strength of singularity
ϕ = outer representation of pertubation potential
ϕ^* = inner representation of perturbation potential
Φ = velocity potential
Ω $=\omega c/U\delta^2$
ω = characteristic frequency

Subscripts

B = body
inner = refers to near field
outer = refers to far field

Special Symbols

$\partial/\partial n$ = normal derivative to contour C referred to in Eq (7b)

Introduction

DURING the 1950 s techniques were developed to analyze and design aircraft to accelerate through what was then called the sound barrier The procedure employed was an area rule' [1] in which the drag of a complete airplane was computed from that of an equivalent body of revolution A related development was the Oswatitsch equivalence rule[2] which was later further developed by Spreiter and Heaslet in Ref 3

In the supersonic Prandtl Glauert regime the equivalent body of revolution flow can be modeled as a linear line

Presented as Paper 83 0184 at the AIAA 21st Aerospace Sciences Meeting Reno Nev Jan 10 13 1983; received Feb 14, 1983; revision received Nov 18 1983

Member of Technical Staff Associate Fellow AIAA
†Associate Research Physicist
‡Professor Fellow AIAA

source The Jones procedure[4] and the ideas embodied in Hayes' equivalence theorem[5] have been used by industry on a routine basis for many years to perform drag estimation and optimization of supersonic shapes Application of the linear line source model to transonic configurations can lead to inaccurate drag predictions and suboptimal arrangements because of important nonlinear effects A more appropriate approach is to determine the drag from a transonic solver for the equivalent body of revolution component of the flow Extensions of the zero lift equivalence rule to treat lift effects and not so slender shapes have been investigated by Cheng and Hafez[6] and Barnwell [7] Evaluations of the validity of the rule have been made by Agrell et al [8] Sedin et al [9] and Chan [10] From the studies of Sedin and Chan there appears to be evidence that the equivalence rule can be used to quantify the drag rise of fighter configurations with wings of moderate thickness ratio Although further studies are required to make the precise range of its applicability more clear it is evident that for many practical shapes, the Oswatitsch rule can provide a powerful method for devising low drag transonic arrangements However the accomplishment of this objective requires a systematic procedure to eliminate or minimize the wave drag of the equivalent body of revolution An example would be constrained minimization [11] which has provided a useful means of optimizing transonic shapes under certain circumstances The design or inverse procedure as exem plified for wings in Ref 12 represents another method which is less computationally intensive Here shapes are sought supporting preassigned pressure distributions in contrast to the direct or analysis method where the reverse is true A typical implementation is to smooth out jump discontinuities in the surface pressure distribution that would be associated with shocks

Use of the equivalence rule and inverse capability opens up attractive possibilities in regard to slender airplane op timization One possibility described here is to apply the technology to the equivalent body of revolution component Since the wave drag arises solely from this contribution a potent means of improving aerodynamic performance is available with simplified versions of modern computational methods Here, the reduction in complexity arises from the dominant axial symmetry of the asymmetric slender body problem in the nonlinear part of the flow

Similar reductions in complexity are also possible in an unsteady transonic framework Here there is interest in obtaining quick procedures such as those developed in Refs 13 and 14 for purposes of assessing aeroelastic and structural dynamic characteristics at near sonic Mach numbers

In this paper results of two investigations involving transonic slender body theory and the equivalence rule will be summarized Further details are given in Ref 15 In the first an unsteady equivalence rule has been developed which can provide useful unsteady aerodynamic inputs for transonic flutter analyses Here, the far field (outer) solution is governed by axisymmetric unsteady small disturbance theory subject to an unsteady line source internal boundary con dition As in the steady case the strength of the line source depends on an inner solution for the potential which is harmonic in cross planes to the flow This solution specifies the line source intensity in terms of a rate of change of the cross sectional area distribution in which the unsteady motion of the body surface is taken into account Some of these concepts have been introduced by Cheng and Hafez in Ref 16 In contrast to that analysis the treatment here will provide a limit process expansion framework This gives an asymp totically precise systematic approximation procedure capable of refinement Moreover the application of the rule for the calculation of unsteady loads will be indicated

The second portion of the research effort described deals with optimization of slender lifting wing body combinations in accordance with previously mentioned ideas A restricted class of these shapes has been considered in which the wing span increases monotonically from a common apex with the body For pointed tails it is shown that the aerodynamic efficiency can be maximized by minimization of the wave drag of the equivalent body of revolution of the wing body A parameterized inverse (PI) procedure is utilized to demon strate substantial decreases in this quantity from the nonlinear equivalent body problem The PI method employs a parameterized fairing of the surface pressure distribution about a discontinuous one associated with a surface shock where the fairing parameters are adjusted to achieve closure or other constraints such as fixed maximum thickness

Analyses

Unsteady Equivalence Rule

For purposes of studying transonic slender asymmetric configurations in unsteady flow the method of matched asymptotic expansions has been used The viewpoint is similar to the steady case Away from the body the flow is nearly axisymmetric and to dominant order a nonlinear line source Near the body, transverse gradients dominate those in the streamwise direction and the flow is linear For low frequency motions a stretched time scale must be used to resolve the nonlinear flow structures The relationship of this time scale to the other parameters, such as the fineness ratio is deter mined from matching the near and far fields Also obtained from this process are the magnitudes of the flow per turbations in both regions In what follows the basic results of the analysis leading to an unsteady equivalence rule are summarized Details of the arguments are given in Ref 15

Basic Equations

Referring to the configuration defined in Fig 4 with the indicated coordinate system and the X axis aligned with the freestream direction the full potential equation in these coordinates is

$$(a^2-\Phi_X^2)\Phi_{XX}+(a^2-\Phi_R^2)\Phi_{RR}+\frac{a^2\Phi_R}{R^2}+\left(a^2-\frac{\Phi_\theta^2}{R^2}\right)\frac{\Phi_{\theta\theta}}{R^2}$$

$$-2\Phi_X\Phi_R\Phi_{RX}-\frac{2\Phi_X\Phi_\theta\Phi_{\theta X}}{R^2}-\frac{2\Phi_\theta\Phi_R\Phi_{\theta R}}{R^2}$$

$$-2\Phi_R\Phi_{TR}-2\Phi_X\Phi_{TX}-\frac{2}{R^2}\Phi_\theta\Phi_{T\theta}-\frac{2\Phi_\theta^2\Phi_R}{R^3}-\Phi_{TT}=0 \quad (1)$$

where the upstream conditions have been assumed to be in dependent of time and subscripts denote partial differentia tion

In Ref 15 near field (inner) and far field (outer) representations for Φ are determined based on Eq (1) the boundary conditions and asymptotic matching procedures These are an unsteady generalization of that given in Refs 17 and 18 Near the body the appropriate inner expansion is

$$\Phi_{\text{inner}}=U\{X+c[(\delta^2\log\delta)2S(x\,\tilde{t})$$

$$+\delta^2\phi(x\,r^*\,\tilde{t}\,K\,\Omega)+\quad]\} \quad (2)$$

where Eq (2) holds in the inner limit

$$x=\frac{X}{c}\quad r^*=\frac{R}{\delta c}\quad \tilde{t}=\delta\frac{2UT}{c}\quad K=\frac{1-M_\infty^2}{\delta^2}$$

$$\Omega=\frac{\omega c}{U\delta^2}\quad \text{fixed as}\quad \delta\to 0 \quad (3)$$

In Eq (2) the function $S(x\,\tilde{t})$ the strength of the line source is related to the body cross sectional geometry which is given by

$$B=R-\delta cF(X\,\theta\,\tilde{t};\ \Omega\,a)=0 \quad (4)$$

where a is an amplitude parameter and $x=X/c$ As an illustration, for a harmonically pitching or plunging body

$$F=ax^n \sin \Omega\tilde{t} \sin\theta + [G^2(x\,\theta) - a^2x^{2n} \sin^2\Omega\tilde{t} \cos^2\theta]^{1/2}$$

where G is the cross sectional shape in the plunging or pitching body axes, $n=0$ for plunge, and $n=1$ for pitch For Eq. (4), then,

$$S(x\,\tilde{t}) = \frac{1}{2\pi}\frac{\partial A}{\partial x} \tag{5}$$

where $A = \frac{1}{2}\oint F^2 d\theta$, and the line integral is around the contour C given by $r^* = F(\theta\, x_0)$ in a plane $x=x_0$ If $r^*=F(\theta\, x)$ is a single valued function of θ

$$A = \frac{1}{2}\int_0^{2\pi} F^2 d\theta$$

A multipole representation for the complete inner solution can then be written as

$$\phi^* = S(x\,\tilde{t})\log r^* + g^*(x\,\tilde{t}) + \sum_{n=1}^{\infty} \frac{g_n(x\,\tilde{t})\cos n\theta + f_n(x\,\tilde{t})\sin n\theta}{r^{*n}} \tag{6}$$

where the coefficients g_n and f_n in Eq (5) are determined from the solution of the boundary value problem

$$\phi^*_{r^*r} + \frac{\phi^*_{r^*}}{r^*} + \frac{1}{r^{*2}}\phi^*_{\theta\theta} = 0 \tag{7a}$$

$$\left.\frac{\partial\phi^*}{\partial n}\right|_{r=F} = \frac{FF_x}{\sqrt{F_\theta^2+F^2}} \qquad 0<x<1 \tag{7b}$$

For the problem embodied in Eqs (7), ϕ^* has the asymptotic behavior given by Eq (6) as $r^*\to\infty$ The function $g^*(x\,t)$ is determined from the solution of a problem for the outer representation of the perturbation potential which has the form

$$\Phi_{\text{outer}} = U\{X + c\delta^2\phi(x\,\tilde{r}\,\tilde{t};K\,\Omega) + \quad\}$$

which is valid in the limit

$$x\,\tilde{r} = \frac{\delta R}{c} \qquad \tilde{t}\;K\;\Omega \text{ fixed as } \delta\to 0$$

The problem for ϕ is

$$[K-(\gamma+1)\phi_x]\phi_{xx} + \frac{1}{\tilde{r}}(\tilde{r}\phi_{\tilde{r}})_{\tilde{r}} - 2\phi_{x\tilde{t}} = 0 \tag{8a}$$

$$\lim_{\tilde{r}\to 0} \tilde{r}\phi_{\tilde{r}} = S(x,\tilde{t}\;N\;\Omega) \qquad 0<z<1 \tag{8b}$$

On the wake, $x>1$, the boundary condition

$$\phi_{\tilde{r}}(x,0\;\tilde{t}) = 0 \tag{8c}$$

holds From the solution of Eq (8), the function g in Eq (6) is given by

$$g = \lim_{\tilde{r}\to 0}\{\phi(x\,\tilde{r}\,\tilde{t}) - S(x\,\tilde{t})\log\tilde{r}\} \tag{9}$$

From the energy invariant and isentropy, the surface pressures on the body $r^*=F$ are given by

$$-\frac{C_p}{\delta^2} = 4(\log\delta)S_x(x\,\tilde{t}) + 2\phi^*_x + v_B^2 + w_B^2 \tag{10}$$

where c has been assumed to be unity and

$$v_B = \frac{S}{F} - \sum_{n=1}^{\infty}\frac{g_n\cos n\theta + f_n\sin n\theta}{F^{(n+1)}} \tag{11a}$$

$$w_B = \sum_{n=1}^{\infty}\frac{n\{-g_n\sin n\theta + f_n\cos n\theta\}}{F^n} \tag{11b}$$

in which g_n and f_n are functions of x and $\tilde{t}$

For an axisymmetric body $r^*=F(x)$ an alternate expression for the surface pressure can be obtained from the outer solution This gives

$$-\frac{C_p}{\delta^2} = 2S_x(x\,\tilde{t})\log\delta^2 F + 2g_x(x\,\tilde{t}) + F^{\,2} \tag{12}$$

Equations (5), (9), and (10) and the backup relations given herein constitute the transonic unsteady equivalence rule In a practical application, a numerical procedure based on this rule can be utilized to compute transonic unsteady flows over low aspect-ratio configurations such as fighter arrangements Its principal simplifying feature in complementing more computationally intensive procedures is that it reduces the three-dimensional problem for Eq. (1) to a pair of two dimensional ones One of these can be treated by simple linear methods The second can be handled by an axially symmetric generalization of time marching algorithms for the unsteady small-disturbance equation for planar flows To obtain a truly useful tool, however generalizations are required to handle shapes in which the wings are non monotonically increasing in span from the nose of the wing body arrangement For these cases the wakes play an important role, modifying the autonomy of downstream sections As in steady interactions, the higher order matching is important including a theory of the materialization of shocks in the near field

Steady Slender Body Theory and Optimization Studies

The previous results when specialized to steady flow can be used to study L/D optimization of a wing body configurations of the type shown in Fig 1 Here the body has a circular cross section; the wing increases monotonically from the pointed apex to the base section and is of zero thickness Based on Refs 17 and 19 the aerodynamic efficiency L/D is given in terms of the vortex drag D_v by

$$\frac{L}{D} = \frac{\pi\delta^2(b^2 - r_0^2 + r_0^4/b^2)\alpha}{\delta^4(B+1) + D_v/\rho_\infty U^2} \tag{13}$$

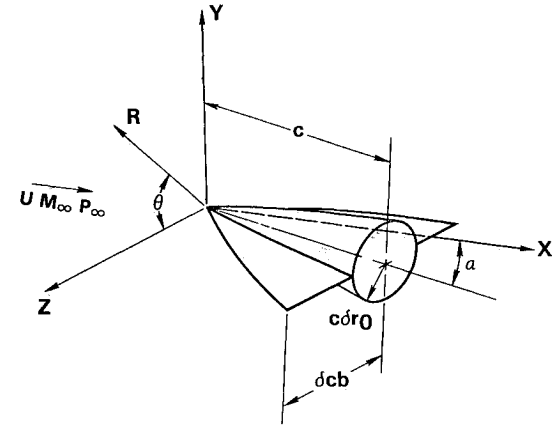

Fig 1 Slender body geometry

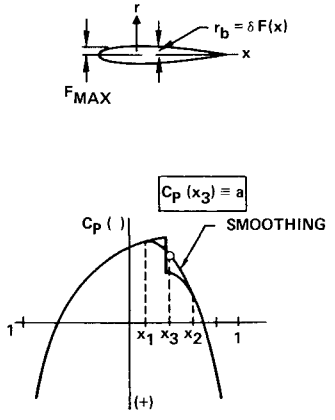

Fig 2 Fourth order smoothing used for refairing shocked surface pressure distributions

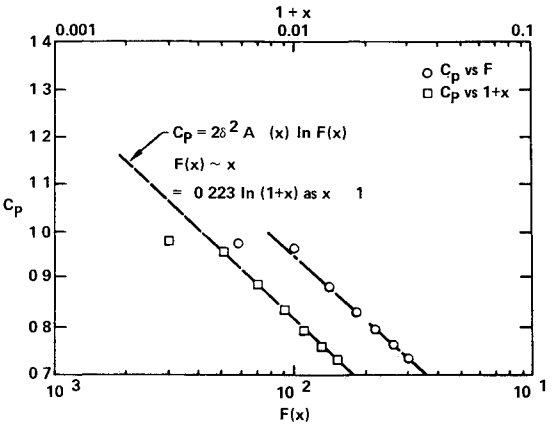

Fig 3 Singular behavior at the nose of a fore and aft symmetric parabolic body $M_\infty = 0\ 98$, $\delta = 0\ 167$ (from SLOR solution)

where

$$B = \pi S(1)g(1) - \frac{1}{2}\int_0^{2\pi} \phi^*(1\ F\ \theta)FF_x(1\ \theta)\,d\theta$$

$$-[\log\delta][2\pi S^2(1)]$$

$$I = -2\pi\int_0^1 S(x)g\ (x)\,dx$$

For $r_0 \neq 0$ care must be taken in applying the proper model for the vortex sheet associated with the body Once this is established D_v can be calculated from the kinetic energy of the vortex system of the wing body arrangement in the Trefftz plane

One procedure considers the body vortex system as a pair of concentrated trailing vortices with potential flow outer regions and viscous solid body rotating cores A purely in viscid pair leads to a nonexistent integral representing the body wake kinetic energy For $r_0 = S(1) = 0$ Eq (3) specializes to

$$\frac{\delta L}{D} = \frac{A}{A^2/2 + (I/\pi b^2)} \tag{14}$$

The first term in the denominator corresponds to the vortex drag which to this order is independent of the body shape and wing planform The second term is associated with the area rule representation of the wave drag in terms of the longitudinal area progression

From Eq (14) it is evident that for the class of con figurations considered minimization of the quantity I using a favorable area distribution maximizes L/D at a fixed A This can be achieved with no coupling to the vortex drag To arrive at such minima a "parameterized inverse" method has been developed in which low drag equivalent bodies of revolution can be obtained The low drag is achieved by designing the body shape to support a shockless surface pressure distribution This procedure is different from another one reported in Ref 20 The latter focused on coupling in the boundary conditions peculiar to the present axisymmetric generalization of the two dimensional airfoil problem described in Ref 12 In what follows a description will be given of a new method that provides a treatment of con straints relevant to the L/D optimization problem related to equations such as Eqs (13) and (14) Examples of such constraints are: prescribed base radius and maximum thickness

This 'parametrized inverse" (PI) procedure consists of the following steps:

1) Starting with a known equivalent axisymmetric body $r^* = F(x)$ the analysis boundary value problem as form ulated in Ref 21, consisting of Eqs (5) and (8) is solved for steady flow to obtain a surface pressure C_p given by Eq (12)

2) In general the pressure distribution of Step 1 will have a discontinutiy associated with a shock termination in the supersonic zone A fourth order polynomial is used to "refair" the region in the vicinity of the shock as schematically indicated in Fig 2 In the notation of the figure control points at x_1 and x_2 are shown and continuity of slope and value of C_p is required at these locations Introduced here are two parameters which minimize the drag C_D and obtain closure in the sense that $F(1) = 0$ (A more general case in which $F(1) \equiv F_1$ is prescribed is also discussed in what follows) The first parameter a is the midpoint value of C_p shown in Fig 2, i e $C_p(x_3)$ The second is the intensity μ of the leading edge singularity where for bodies pointed at the nose and tail according to Eq (12)

$$C_{p_b} = \mu\log(1 \pm x) \quad \text{as } x \to \mp 1 \qquad (\text{if } F \sim 1 \pm x)$$

and

$$\mu \sim F^{\,2}(0) \qquad F\ (0) = -F\ (1)$$

Here the subscript b refers to the body value A C_p variation near the nose of a symmetric parabolic arc body illustrating this behavior is shown in Fig 3 where the freestream Mach number $M_\infty = 0\ 98$ and the thickness ratio $\delta = 0\ 167$ It can be seen that the numerical procedure tracks the singularity quite well except at the first mesh point which is understandable In fact the proper strength μ is also obtained on inspection of the slope of the curves and Eqs (5) and (8b)

3) In the iteration procedure a given value of the parameter a is assumed as well as μ The latter is regarded as a constant multiplicative factor for the entire $C_{p_b}(x\ a\ \mu)$ distribution on the interval $-1 \leq x \leq 1$ Regarding Eq (12) as an ordinary differential equation for F in which g_x is assumed to be known from a previous iteration with C_p specified a two point boundary value problem is solved for this equation in which

$$F(0) = 0 \tag{15a}$$

$$F(1) = F_1 \tag{15b}$$

are the boundary conditions With g_x fixed at this stage, the solution technique is the method of bisection coupled with a Runge Kutta integration procedure In the implementation for $F_1 = 0$ two initial values of μ μ_1 and μ_2 are obtained to bound a range where $F(1)$ changes sign Values of μ are changed in the left hand side of Eq (12) using relaxation A

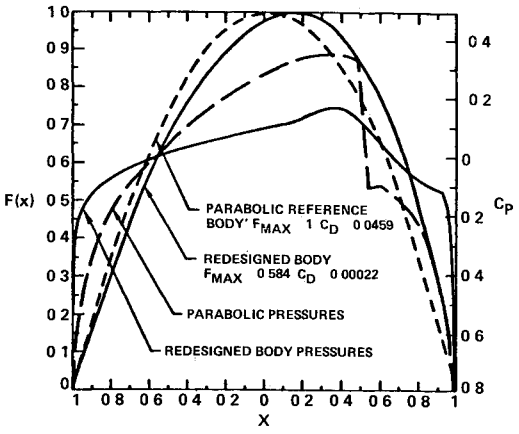

Fig 4 Body redesign: $M_\infty = 0\ 98$ $\delta = 0\ 167$, $K = (1-M_\infty^2)/M_\infty^2\delta^2 = 1\ 48$

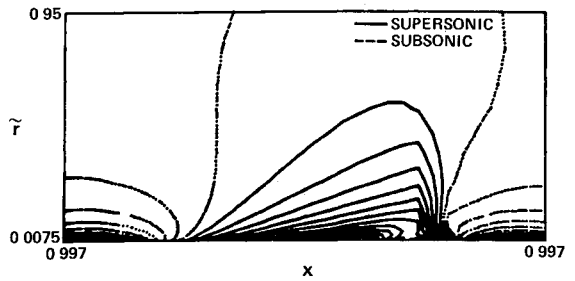

Fig 5 IsoMachs for parabolic reference body

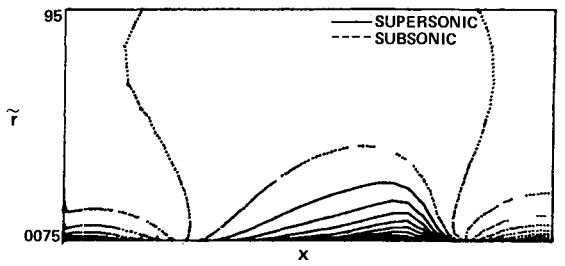

Fig 6 IsoMachs—redesigned body (height of sonic bubble ≈ 0 24)

set of loops are initiated in which if Γ is the relaxation parameter,

$$C_{p_{\text{relaxed}}} = \Gamma C_{p_{\text{old}}} + (1-\Gamma) C_{p_{\text{target}}} \tag{16a}$$

and

$$C_{p_{\text{newer}}} = \mu C_{p_{\text{new}}} \tag{16b}$$

The ordinary differential based on Eq (12) is solved with Eq (16b) and the bisection method until

$$|F(1)| < 0\ 001 \tag{16c}$$

The bisection method also applies to the case where $F_1 \neq 0$ Instead of Eq (16c), the condition is $|F(1) - F_1| < 0\ 001$ Our experience has been that convergence is very rapid with this approach Typical values for the μ_i are 0 2 and $\mu_2 = 1\ 8$

4) Once a new F distribution satisfying Eq (15) is ob tained the analysis algorithm described in Step 1 is used to recalculate C_p and g (x) In this step F is relaxed in ac cordance with the relationship,

$$F_{\text{relaxed}} = \frac{F_{\text{old}} + F_{\text{new}}}{2} \tag{17}$$

5) Steps 3 and 4 are repeated until

$$C_{p_{\text{new}}} = C_{p_{\text{target}}}$$

6) As a means of obtaining a minimum level, the value of the drag coefficient is correlated against other values of the parameter a introduced in Step 3 In Eq (16a) the value of Γ is adjusted in accord with the rule

$$\Gamma = 1 - \frac{n^2}{8+n^2} \tag{18}$$

where $1 < n < 40$, and n = number of iterations Thus ac cording to Eq (18) $\Gamma \to 0$ as $n \to \infty$

7) In a recent development the value of F is renormalized by introducing a new F in accord with the relation

$$F = \frac{F}{F_{\max}} \qquad (F_{\max} \equiv \max_{0 \le x \le 1} F) \tag{19}$$

Step (7) which gives $R_{\max} = 1$ in Eq (4) is integrated into the iteration procedure as a means of introducing a fair basis of comparison of the drag levels

It should be noted that in the successive line overrelaxation (SLOR) analysis code employed in Step 4 it was adequate to use only 15 sweeps before the next phase of the iteration process was initiated

Results

In what follows illustrations of the previously described PI method to obtain shockless pressure distributions and closed axisymmetric bodies will be provided The implications of these measures with respect to wave drag will be considered Also presented are calculations from algorithms devised for the satisfaction of other constraints besides closure e g , $F_1 \neq 0$ in Eq (15b) Viscous effects and base drag on finite base afterbodies have not been addressed here but deserve future consideration Also basic issues of existence and uniqueness deserve attention Another aspect investigated was the attainability of a zero wave drag body of revolution

To show the inverse method's ability to eliminate surface shocks modifications of symmetric parabolic arc bodies were considered initially Figure 4 depicts a vertically expanded version of such a body (dashed curve) The associated pressure (dashed curve) indicates a jump discontinuity produced by a shock at a location downstream of the mid point of the body For these calculations 89 points were used in the x direction with 55 points across the body In the r direction 31 points were employed Clustering was used in the vicinity of the nose and tail of the body for the x grid and the usual expansion of the r grid at large distances from the axis of symmetry was also applied A smoothed pressure distribution shown here by the solid curve arises from the 4th order polynomial discussed previously where the hump is indicative of the solution for the parameter a required to achieve closure The closure of the redesigned body also shown by the solid curve is typical of the success we have had with the PI procedure in meeting this goal

Although wave drag reduction can be achieved by smoothing the surface pressures wave envelopes may arise off the body These discourage complete wave drag elimination Accordingly it is of crucial interest to establish under what conditions such envelopes form and more im portantly when removal of the surface pressure discontinuity results in zero drag In this connection it should be noted that solutions of Ref 20 as well as the PI method of this paper produce reduced but finite wave drag with smoothed surface pressure distributions In Ref 20 the issue of closure was not

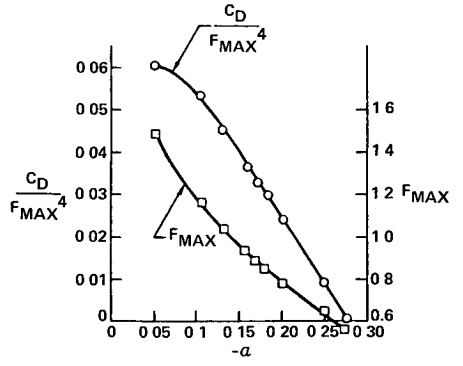

Fig 7 Wave drag and EBR maximum thickness F_{max} vs surface C_p smoothing parameter, a

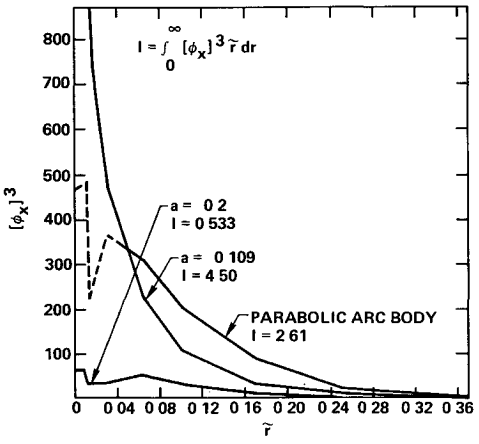

Fig 8 Entropy jump shock drag for various bodies

addressed Subcritical cases discussed therein demonstrated a finite drag for unclosed bodies Since a finite base body violates the assumptions in the usual proofs of D' Alembert's paradox this result should be studied Because the bodies can be closed in the PI method the wave drag can be traced directly to the shock system

Regarding the issue of drag the basic drag coefficient C_D of the parabolic body for the case of Fig 4 was computed to be 0 0459 For the refaired pressure distribution obtained in the iterations of the PI method convergence to a value of $a = -0\ 1275$ led to $C_D = 0\ 00022$, practically zero to within the truncation error of the calculations This result is tempered by the reduction of F_{max} from unity for the parabolic case to a value of 0 524 in the refaired case Since there is a natural reduction in drag with thickness ratio, a fair comparison between the original and designed body should really be performed with both at the same thickness The drag of the rescaled redesign is obtained using the transonic similarity rule which for axisymmetric bodies of thickness ratio δ is

$$\tilde{C}_D \equiv \frac{C_D}{\delta^4} = f(K) \tag{20a}$$

where

$$K = (1 - M_\infty^2)/\delta^2 \tag{20b}$$

Accordingly if a C_{D_l} is associated with an $F_{l_{max}} = \mu$ and $\mu < 1$ then the body thickness ratio should be increased by a factor μ^{-1}, and a new drag coefficient C_{D_2} should be calculated from a new analysis solution to evaluate $f(K_2')$ where $K_2' = \mu^2 K_l'$ It follows that

$$C_{D_2} = \frac{1}{\mu^4} f(\mu^2 K_l') \tag{21}$$

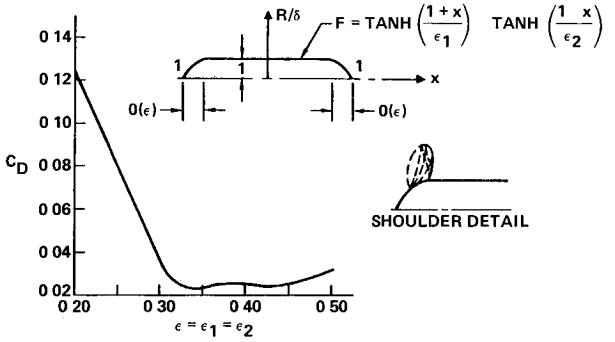

Fig 9 Wave drag of nearly cylindrical bodies

is the appropriate comparison drag coefficient for the blown up redesigned body Since the rescaling of K_2' to $\mu^2 K_l'$ drastically changes the flow field with a probable generation or intensification of shocks for $\mu < 1$ it is important to implement Step 7 in the PI procedure previously described if a meaningful drag reduction is to be achieved Some results of preliminary efforts of this direction will be described subsequently The procedure described in Ref 20 embodies the feature of renormalizing F_{max} during its iteration cycle

As a basis for a different sort of standardized comparison the flow field over a reference parabolic arc body with $F_{max} = 0\ 524$ was computed at $K^* \equiv (1 - M_\infty^2)/M_\infty^2 \delta^2 = 1\ 48$ the value utilized for the original parabolic and the redesigned body In contradistinction to the redesigned body the parabolic body had a shock discontinuity on its surface Although the drag for the parabolic shape is low ($C_D = 0\ 00066$), it is still three times larger than the redesigned contour's

Since the emphasis in the PI method is to achieve closure, as well as to address the question of the existence of drag free bodies at transonic speeds the issue of F_{max} standardization is of lesser importance at this stage of the discussion The significance of the redesign of Fig 4 can be more fully appreciated from a picture of the flow above the body Such pictures are provided herein in terms of isoMach lines In Fig 5, the isoMach pattern for the parabolic reference body at the conditions of Fig 4 is indicated The solid lines indicate supersonic regions and the dashed lines signify subsonic zones In the map, the concentration of contours above the 75% location of the body associated with the shock and the transition from supersonic to subsonic flow at the shock is evident

By contrast to the shocked pattern evident in Fig 5 Fig 6 indicates a shock free mixed flow Thus, in spite of the F_{max} reduction these figures provide some insight into the question of whether drag free bodies of revolution exist in mixed flow On the basis of the apparent shock free nature of the flow field and the extremely low drag value $C_D = 0\ 00022$ prospects would appear encouraging for finding such bodies The PI method appears to provide an attractive procedure for generating such closed shapes To further elucidate the relevant drag controlling mechanisms the nonlinear axisymmetric hodograph is linear Garabedian[22] solves it numerically while Nieuwland[23] provides analytical solutions In some sense these treatments prove the existence of shock free airfoils Due to the nonlinearity of the hodograph for the axisymmetric case existence of shock free bodies can probably be demonstrated in a constructive sense only i e the numerical solution of the boundary value problem in the hodograph plane

It is also interesting to note that Fig 4 shows that the point of maximum thickness moves rearward for drag reduction in mixed flow over a body This is in agreement with the optimum supersonic airfoil which is a vertically symmetric wedge section whose maximum thickness moves aft with increasing Mach number

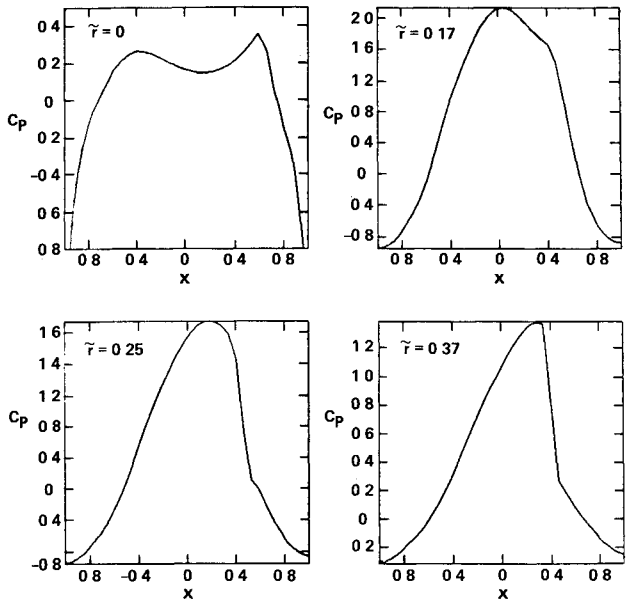

Fig 10 Development of C_p vs x at various levels above tanh body

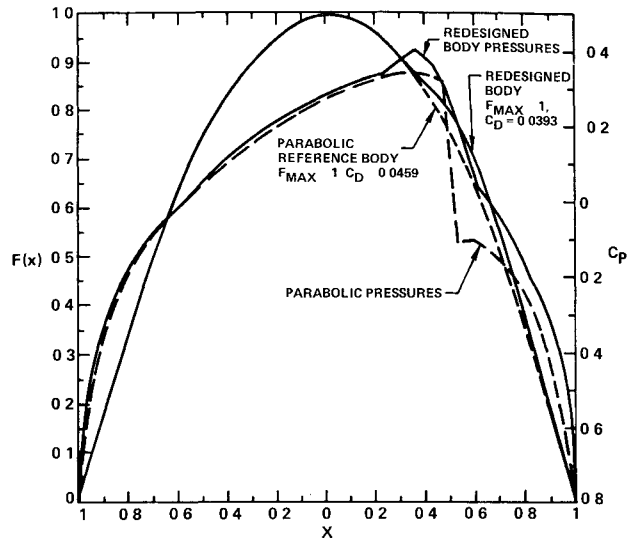

Fig 11 Body design with $F_{max}=1$ constraint and closure implemented

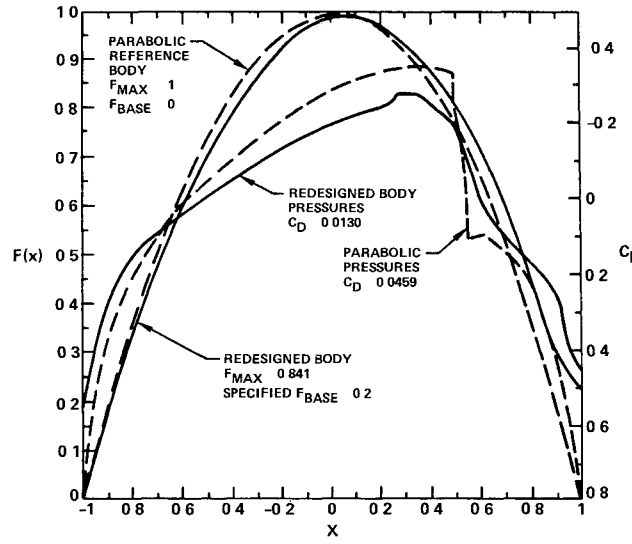

Fig 12 Parametrized inverse method successfully applied to base constraint

Returning to Fig 4 a study of the sensitivity of the drag due to the fairing parameter a was conducted The results are shown in Fig 7 where C_D and F_{max} are plotted vs $-a$ A systematic trend is indicated showing that potent gains can be achieved through the use of relatively simple minded smoothings of the shock discontinuities

In a previous treatment of the optimization problem for bodies of revolution Chan[24] treated a two parameter family of general parabolic bodies of the form $S(x)=Ax^n(1-x)^m$ $A=(n+m)^{(n+m)}/8n^n m^m$ using numerical optimization to determine the best selection of n and m to minimize the drag As in most optimization procedures, the best selection of n and m did not eliminate the drag and provided only a local minimum In the PI procedure, there appears to be an opportunity to exercise some control over the drag directly through the shock smoothing mechanism mentioned previously Yet as already indicated no control of the wave drag related envelope formation off the body has been exercised in the current PI implementation

Another study of wave drag associated with various values of the parameter a is shown in Fig 8 where the entropy jump integral across the shock (which is proportional to the wave drag) is shown Dramatic differences are demonstrated in which a fairing parameter $a=-0\ 109$ can be selected to give a drag actually higher than that of the parabolic body Also indicated is a very small value associated with $a=-0\ 2$ In the figure the indicated irregularities are associated with the usual difficulties of shock capture

In studying the optimization process the question of whether the parabolic body is a disadvantageous initial iterate for PI process becomes important The thrust of the question pertains to the possibility that flattened bodies such as supercritical airfoils are useful as drag reducers since their slope contributions to the wave drag integral are nearly zero on their nearly cylindrical portions The associated shocks could also be weak due to suppression of the envelope of the reflections One candidate for consideration is the shape shown in Fig 9 hereafter referred to as the tanh body In spite of the deleterious effect of overexpansions near the forebody shoulder and the resulting shock the drag can be minimized to about one half of the parabolic value through the selection of the parameter ϵ the effective forebody length It is interesting to note that $\epsilon=0\ 12$ gives about three times the parabolic body result for the tanh shape

As an illustration of some of the nonlinear wave steepening mechanisms present Fig 10 shows a sequence of axial distributions of pressure at various heights above the body The results are plotted for the minimum drag value of ϵ The impossibility of improvement stems from the overtaking of the expansion compression hump over the afterbody shoulder by another hump from the forebody shoulder As the height increases the latter swallows up the former At even greater heights a mild shock forms The shock was detected in this case by monitoring finite jump discontinuities of ϕ_{xx} and using expanded scales in graphic visualizations of the process

To demonstrate the implementation of Step 7 in the PI method the case of Fig 6 was run again in which the parameter $a=-0\ 17$ In Fig 11 the body solution is shown as the indicated bulge about the parabolic contour Figure 11 indicates pressures for original and redesigned contour A substantial drag reduction is indicated although the smoothing on the body evidently does not eliminate wave drag which presumably is due to shocks off the body This envelope process should be studied carefully in future efforts

In connection with earlier remarks on L/D the last example shown in Fig. 12 illustrates the use of the PI procedure for a constrained finite base As previously the reference parabola is indicated for comparison purposes The

associated refaired pressure distribution is indicated in the figure The more sizable drag reductions indicated can be ascribed partially to the relaxation of the $F_{max} = 1$ constraint and the resulting diminution of F_{max} Actually, this can form the basis of a tradeoff of stored volume and wave drag In the implementation for the finite base case, the absence of the tail singularity was ignored, with no major effect on the con vergence of the closure iteration loop. Worthy of mention here, is the subtle distinction between a sting support open body wake, and finite base For the first second, and fourth situations a tail singularity is possible For the third though it is unlikely

Conclusions

For unsteady flows analytical results have been provided that indicate the existence of an unsteady equivalence rule Just as in the steady case, the three dimensional nonlinear problem for slender shapes can be simplified to an axiysm metric one, with internal boundary conditions associated with asymptotic behavior of an inner solution which is harmonic in cross planes With the substantial current cost of computing transonic unsteady flows as well as the need for avoiding non classical flutter, the simplifications and cost reductions afforded by such a rule could be of substantial advantage

In the steady case for certain classes of wing body com binations in which the wing is of zero thickness and increases its span monotonically from a common apex the L/D op timization problem consists of minimizing the drag of the body for a fixed span of the wing Furthermore if the body is pointed the wing body interference lift has been shown by previous investigators to be equal to that of the isolated wing For the drag minimization process associated with these lifting wing body combinations, it is now clear that the PI method discussed here can provide an extremely useful tool

Substantial reductions of the wave drag can be achieved in many cases where the surface jump discontinuity is refaired It has also been demonstrated that the refairing process can be utilized to achieve satisfaction of constraints such as closure and fixed maximum thickness However there are certain situations in which shocks develop off the body These have been demonstrated in our effort For these cases, the elimination of a surface discontinuity may reduce the wave drag but not completely eliminate it Therefore a knowledge of the theory of characteristic propagation and envelope formation for flow over axisymmetric bodies could provide target surface pressures to eliminate these off body shocks Other aspects of the research have shown that the initial iterate in the design process can play a role in the degree of possible drag minimization In fact a study of a nearly cylindrical body when optimized in its forebody and af terbody sections provides substantial reductions from the symmetric parabolic shape if the lengths of the sections are optimized As has been previously discussed the role of overexpansions and shock formation is intimately involved in the proper adjustment of these lengths

Acknowledgment

Research was sponsored by the Air Force Office of Scientific Research (AFSC) United States Air Force, under Contract No F49620 80 C 0081 The United States Government is authorized to reproduce and distribute reprints for governmental purposes notwithstanding any copyright notation thereon

References

[1] Whitcomb R T , A Study of the Zero Lift Design Drag Rise Characteristics of Wing Body Combinations Near the Speed of Sound NACA Rpt 1273 1952

[2] Oswatitsch K and Kuene F Ein Aquivalensatz fur Nichtangestellte Fluge Kleiner Spannweite in Schallnaher Stromung *Zeitschrift fur Flugwissenschaften* Vol 3 No 2 Feb 1955 S 29 46

[3] Heaslet M A , and Spreiter, J R , Three Dimensional Tran sonic Flow Theory Applied to Slender Wings and Bodies NACA Rpt 1318 Sept 1956

[4] Jones R T Theory of Wing Body Drag of Supersonic Speeds ' NACA Rpt 1284 1953

[5] Hayes, W D Linearized Supersonic Flow North American Aviation Rpt No AL 222, Los Angeles, Calif 1947

[6] Cheng H K and Hafez M M Transonic Equivalence Rule; a Nonlinear Problem Involving Lift *Journal of Fluid Mechancis* Vol 72 Pt 1 1975 pp 161 187

[7] Barnwell, R W Transonic Flow About Lifting Con figurations " *AIAA Journal* Vol 11, May 1973 pp 764 766

[8] Agrell N Mattsson R and Nyberg, I 'Investigation of the Transonic Drag Characteristics or Non Slender Wing Body Com binations and Their Equivalent Axisymmetric Bodies at Zero Lift *Proceedings of 11th Congress of the International Council of the Aeronautical Sciences*, Vol II, Sept 1978, pp 292 304

[9] Sedin Y C J , Qualitative Calculations of Transonic Drag Rise Characteristics Using the Equivalence Rule *Proceedings of the 11th Congress of the International Council of the Aeronautical Sciences* Vol. II, Sept 1978 pp 71-84

[10] Chan Y Y An Experimental Study of the Transonic Equivalence Rule with Lift, National Research Council of Canada Aeronautical Rpt LR-609 NRC 20225 March 1982

[11] Hicks, R M , and Henne, P A Wing Design by Numerical Optimization AIAA Paper 77 1247 1977

[12] Shankar V Malmuth N D and Cole J D , Computational Transonic Inverse Procedure for Wing Design *AIAA Journal* Vol 8 Aug. 1982 pp 1044 1050

[13] Malmuth N D Cole J D Chakravarthy S , and Goebel T P 'Investigation of Structural Dynamic Instabilities in Transonic Flow ' Contract F3315 80 C 3208, Air Force Wright Aeronautical Laboratories Final Rept AFWAL TR 82 3003 Feb 1982

[14] Malmuth, N D Chakravarthy S R Cole J P and Goebel T P Bending Effects on Structural Dynamic Instabilities of Transonic Wings,' AIAA Paper 83 0920 May 1983

[15] Malmuth N D , Cole J D Wu C D , and Zeigler F , Transonic and Nonlinear Flow Research Air Force Office of Scientific Research Final Rept Rockwell Rept No SC5267 3FR May 1982

[16] Cheng H K and Hafez M M Equivalence Rule and Transonic Flows Involving Lift U S C School of Engineering Rept USCAE 124 April 1973

[17] Cole J D Studies in Transonic Flow I Transonic Area Rule Bodies UCLA Rept UCLA Eng 7257, Aug 1972

[18] Cole, J D , Studies in Transonic Flow IV—Unsteady Transonic Flow, UCLA Rept UCLA Eng 76104 Oct 1976

[19] Ashley H and Landahl, M *Aerodynamics of Wings and Bodies* Addison Wesley Reading Mass 1965

[20] Shankar V Numerical Boundary Condition for the Transonic Axisymmetric Inverse Problem *Proceedings of Symposium on Numerical Boundary Condition Procedures* NASA CP2201 Oct 1981

[21] Krupp J A and Murman, E M , 'Computation of Transonic Flows Past Lifting Airfoils and Slender Bodies ' *AIAA Journal* Vol 10, July 1972, pp 880 886

[22] Garabedian P R and Korn, D G Numerical Design of Transonic Airfoils *Numerical Solution of Partial Differential Equations—II* Academic Press New York 1971

[23] Nieuwland, G Y 'Transonic Potential Flow Around a Family of Quasi Elliptical Airfoil Sections National Luchten Ruimfevaart Laboratorijm Amsterdam, NLR TR T 172 1967

[24] Chan Y Y Mundie D L , and Jones D J Transonic Axisymmetric Bodies with Minimal Wave Drag *Canadian Aeronautics and Space Journal* Vol 26 No 3 1980 pp 231 234